Dynamics of a closed rod with twist and bend in fluid

Sookkyung Lim [*] Anca Ferent [†] X. Sheldon Wang [‡] Charles S.Peskin [§]

Abstract

We investigate the instability and subsequent dynamics of a closed rod with twist and bend in a viscous, incompressible fluid. A new version of the immersed boundary (IB) method is used in which the immersed boundary applies torque as well as force to the surrounding fluid and in which the equations of motion of the immersed boundary involve the local angular velocity as well as the local velocity of the fluid. An important feature of the IB method in this context is that self-crossing of the rod is automatically avoided because the rod moves in a continuous (interpolated) velocity field. A rod with a uniformly distributed twist that has been slightly perturbed away from its circular equilibrium configuration is used as an initial condition, with the fluid initially at rest. If the twist in the rod is sufficiently small, the rod simply returns to its circular equilibrium configuration, but for larger twists that equilibrium configuration becomes unstable, and the rod undergoes large excursions before relaxing to a stable coiled configuration.

Key words. equilibria, supercoiling, immersed boundary method, Kirchhoff theory
AMS subject classifications. 65-04, 65M06, 76D05, 76M20

1 Introduction

Supercoiling (writhing) dynamics are observed, for example, in the structural deformation of DNA [29, 30, 31] and in the growth of filaments of bacteria *Bacillus Subtilis* [22, 23, 24]. The overwound or underwound double helix of DNA occurs in DNA transcription, DNA replication, and formation of DNA loops in protein-DNA interactions, which are essential in biological processes. The rod-shaped bacterium *B. Subtilis* elongates, and then divides and separates as it grows, but some cells fail to separate, and this results in supercoiling of the chain of attached bacteria.

Kirchhoff's rod model has been employed to study these biomechanical phenomena. The Kirchhoff model describes the rod as a three-dimensional space curve accompanied by an orthonormal triad (material frame, not to be confused with the Frenet frame of differential geometry)

[*]Mathematical Biosciences Institute, Ohio State University, 231 West 18th Ave., Columbus, OH 43210. Present address: University of Cincinnati, 839 Old Chem, Cincinnati, OH 45221 (limsk@math.uc.edu)

[†]Courant Institute of Mathematical Sciences, New York University, 251 Mercer St., New York, NY 10012 USA and INRIA, 78153 Le Chesnay, France (ferent@cims.nyu.edu)

[‡]Department of Mathematical Sciences, New Jersey Institute of Technology, 323 Martin Luther King, Jr. Blvd. Newark, NJ 07102 (xwang@njit.edu)

[§]Courant Institute of Mathematical Sciences, New York University, 251 Mercer St., New York, NY 10012 (peskin@cims.nyu.edu).

at each point that keeps track of the local orientation of the material. The theory of Kirchhoff for a thin elastic rod [7] has been developed to find stable and unstable equilibrium configurations and to analyze the dynamics of the supercoiling instability, with or without taking into account self-contact forces. The study of a bent and twisted rod can be performed either in the absence of fluid [4, 6, 14, 15, 16, 17, 19, 31, 33] or in the presence of fluid [3, 13, 32] in which the rod is immersed.

One of main issues in modeling supercoiling phenomena is *self-contact*, in which one point of the rod touches another point on the rod. It is usually necessary in this situation to prescribe self-contact forces which do not allow the rod to pass through itself.

In this paper we focus on the supercoiling instability of a circular rod in a viscous fluid. We consider an elastic circular rod with an initially uniform twist that adds up to an integer number of full turns so that the triad configuration of our material frame is smoothly periodic. (The restriction to an integer number of turns is not a fundamental one in the case of a rod with circular cross section, but we make that restriction anyway to avoid dealing with a material frame described by a multivalued triad.) The rod is assumed to be isotropic, homogeneous, and embedded in a viscous incompressible fluid. We represent the rod as a space curve, and we keep track of the orientation of an orthonormal triad (material frame) at each point of the space curve so that we may know how much the rod twists or bends. The triad rotates at the local angular velocity of the fluid, and applies torque locally to the fluid.

In the standard Kirchhoff rod model, the material frame is not independent of the space curve that defines the centerline of the rod. In particular, one of the vectors of the triad is constrained to be tangent to the space curve. Another constraint that is normally imposed on the Kirchhoff rod model is that of inextensibility: the rod can bend and twist, but it cannot stretch. Because of the no-slip condition at the boundary of a viscous fluid, these constraints imply rather complicated boundary conditions in a fluid in which the rod is immersed. In particular, inextensibility requires $\boldsymbol{\tau} \cdot (\boldsymbol{\tau} \cdot \nabla \mathbf{u}) = 0$, where $\boldsymbol{\tau}$ is the unit tangent to the rod and $\mathbf{u}$ is the velocity field of the fluid, and keeping the triad aligned with the rod requires $(\nabla \times \mathbf{u}) \times \boldsymbol{\tau} = \boldsymbol{\tau} \cdot \nabla \mathbf{u}$. These conditions on the fluid velocity field need to be imposed along the space curve that defines the position of the rod. In this paper, however, we avoid these constraints on the fluid velocity by allowing the rod to stretch and also by allowing the orientation of the triad to deviate from alignment with the direction of the space curve. Instead of imposing the above constraints exactly, we postulate an elastic energy function which tends to maintain them. Thus, our rod is allowed to stretch slightly, and our triad is allowed to deviate slightly from the alignment with the tangent direction to the rod.

The immersed boundary (IB) method [25] is used to analyze the dynamics and the instability of a closed circular rod with twist and bend in fluid. The IB method was created to study fluid dynamics of heart valves [26, 27, 28] and has been applied to many problems mostly in biofluids [9, 8, 11, 12, 18, 20, 34]. The present work requires a significant generalization of the IB method because of the need to evaluate the local angular velocity of the fluid and also the need to apply torque locally to the fluid. A preliminary presentation of the method described here was made in [10].

A particular advantage of the IB method in the present context is that the rod does not go through itself because of the continuity of the interpolated fluid velocity field (see section 3), which means there is no need to add artificial conditions that prevent self-crossing. This is rigorously true in the continuous IB formulation of the problem and remains true in practice if discretization

parameters are appropriately chosen.

In section 2, we describe the balance equations of force and moment, and we discuss the equilibrium configurations of a closed circular rod in a horizontal plane. A sinusoidal perturbation is introduced to study the instability of elastic rods. The sinusoidally perturbed rod, in a fluid at rest, will be used as an initial condition in our simulations. The IB method is both a mathematical formulation and a numerical method that will describe the interaction between a bent, twisted rod and the fluid in which it is immersed. The mathematical formulation will be stated in section 3 followed by the description of the numerical scheme in section 4. In section 5, numerical results concerning equilibria of a closed rod will be discussed. We present various shapes of supercoiled equilibrium configurations depending on an intrinsic twist, perturbation parameter, and the ratio of the bend and twist moduli. The paper concludes in section 6. An Appendix is provided which describes the unconstrained Kirchhoff rod model that is used in this work.

2 Equilibrium configuration of a twisted circular rod

Because of the nonstandard features of our Kirchhoff rod model, as described above, we need to derive the equilibrium configuration of a twisted circular rod. The configuration that we find will be close to the standard one ([21], but see comment below), and will approach the standard equilibrium configuration as the stretch modulus b_3 and the shear force constants b_1 and b_2 all approach infinity. Another purpose of this section is to introduce our rod model, before putting it in fluid, and to state its governing equations.

An elastic rod can be represented by a space curve $\mathbf{X}(s)$ together with an orthonormal director basis $\{\mathbf{D}^1(s), \mathbf{D}^2(s), \mathbf{D}^3(s)\}$ where s is a Lagrangian parameter (not necessarily arclength) along the rod. It is assumed that the rod has a circular cross section with constant radius. The triad $\{\mathbf{D}^1(s), \mathbf{D}^2(s), \mathbf{D}^3(s)\}$ is a material frame at each point of the rod subject to the constraints $\mathbf{D}^i \cdot \mathbf{D}^j = \delta_{ij}, i, j = 1, 2, 3$. In the standard Kirchhoff rod model, one of the triad vectors (usually $\mathbf{D}^3$) is constrained to point in the direction of the tangent vector $\frac{\partial \mathbf{X}}{\partial s}$, but we do not impose this constraint here. Instead we provide forces that tend to keep $\mathbf{D}^3$ aligned with $\frac{\partial \mathbf{X}}{\partial s}$, as described below.

The force $\mathbf{F}$ and moment $\mathbf{N}$ transmitted across a section of the rod can be obtained by averaging the stresses acting across that section. Balance of momentum and angular momentum yield

$$0 = \mathbf{f} + \frac{\partial \mathbf{F}}{\partial s} \tag{1}$$

$$0 = \mathbf{n} + \frac{\partial \mathbf{N}}{\partial s} + \frac{\partial \mathbf{X}}{\partial s} \times \mathbf{F} \tag{2}$$

where $\mathbf{f}$ and $\mathbf{n}$ are force per unit length as measured by the parameter s and torque per unit length as measured by the parameter s applied to the rod, respectively [1, 21]. (Recall that s is not arc length in general. The variables $\mathbf{f}$ and $\mathbf{n}$ are densities with respect to the measure ds.)

The internal force and moment on the perpendicular cross section, $\mathbf{F}$, $\mathbf{N}$, and also the applied

force density $\mathbf{f}$ and the torque density $\mathbf{n}$ may be expanded in the basis $\{\mathbf{D}^1, \mathbf{D}^2, \mathbf{D}^3\}$.

$$\begin{aligned}
\mathbf{F} &= F^1\mathbf{D}^1 + F^2\mathbf{D}^2 + F^3\mathbf{D}^3 && (3)\\
\mathbf{N} &= N^1\mathbf{D}^1 + N^2\mathbf{D}^2 + N^3\mathbf{D}^3 && (4)\\
\mathbf{f} &= f^1\mathbf{D}^1 + f^2\mathbf{D}^2 + f^3\mathbf{D}^3 && (5)\\
\mathbf{n} &= n^1\mathbf{D}^1 + n^2\mathbf{D}^2 + n^3\mathbf{D}^3 && (6)
\end{aligned}$$

and the constitutive relations of the version of the Kirchhoff rod used here are as follows:

$$N^1 = a_1\frac{\partial \mathbf{D}^2}{\partial s}\cdot\mathbf{D}^3, \quad N^2 = a_2\frac{\partial \mathbf{D}^3}{\partial s}\cdot\mathbf{D}^1, \quad N^3 = a_3\frac{\partial \mathbf{D}^1}{\partial s}\cdot\mathbf{D}^2 \tag{7}$$

$$F^1 = b_1\mathbf{D}^1\cdot\frac{\partial \mathbf{X}}{\partial s}, \quad F^2 = b_2\mathbf{D}^2\cdot\frac{\partial \mathbf{X}}{\partial s}, \quad F^3 = b_3(\mathbf{D}^3\cdot\frac{\partial \mathbf{X}}{\partial s} - 1) \tag{8}$$

where a_1 and a_2 are the bending moduli of the rod about $\mathbf{D}^1$ and $\mathbf{D}^2$, respectively, and where a_3 is the twisting modulus of the rod. These moduli are standard in the Kirchhoff rod model. Note that $a_1 = a_2$ in the case of a rod with a circular cross section and axially symmetric material properties. The constitutive equations, Eq. (8), are the means by which we approximately enforce the constraints that $s = \mathrm{arclength}$ and that $\mathbf{D}^3$ should point in the same direction as $\frac{\partial \mathbf{X}}{\partial s}$. As we show in the Appendix, the above unconstrained version of the Kirchhoff rod model can be derived from a variational argument in which we postulate an elastic energy of the form

$$E = \frac{1}{2}\int [a_1(\frac{d\mathbf{D}^2}{ds}\cdot\mathbf{D}^3)^2 + a_2(\frac{d\mathbf{D}^3}{ds}\cdot\mathbf{D}^1)^2 + a_3(\frac{d\mathbf{D}^1}{ds}\cdot\mathbf{D}^2)^2 \tag{9}$$

$$+b_1(\mathbf{D}^1\cdot\frac{d\mathbf{X}}{ds})^2 + b_2(\mathbf{D}^2\cdot\frac{d\mathbf{X}}{ds})^2 + b_3(\mathbf{D}^3\cdot\frac{d\mathbf{X}}{ds} - 1)^2]ds \tag{10}$$

To find an equilibrium configuration of a circular rod in a horizontal plane we introduce cylindrical coordinates (r, θ, z) with unit vectors $(\mathbf{r}(\theta), \boldsymbol{\theta}(\theta), \mathbf{z})$. Recall that

$$\begin{aligned}
\mathbf{r}(\theta) &= (\cos\theta, \sin\theta, 0) && (11)\\
\boldsymbol{\theta}(\theta) &= (-\sin\theta, \cos\theta, 0) && (12)\\
\mathbf{z} &= (0, 0, 1) && (13)
\end{aligned}$$

and $\mathbf{r}'(\theta) = \boldsymbol{\theta}(\theta), \boldsymbol{\theta}'(\theta) = -\mathbf{r}(\theta)$. Let $s = r_0\theta, 0 \le s \le 2\pi r_0$, and then construct the configuration $\mathbf{X}(s)$ and the orthonormal triad $\{\mathbf{D}^1(s), \mathbf{D}^2(s), \mathbf{D}^3(s)\}$ as follows:

$$\begin{aligned}
\mathbf{X}(s) &= r_1\mathbf{r}(s/r_0) && (14)\\
\mathbf{D}^3(s) &= (\cos\beta)\boldsymbol{\theta}(s/r_0) + (\sin\beta)\mathbf{z} && (15)\\
\mathbf{E}(s) &= -(\sin\beta)\boldsymbol{\theta}(s/r_0) + (\cos\beta)\mathbf{z} && (16)\\
\mathbf{D}^1(s) &= \cos(ps/r_0)\mathbf{E}(s) + \sin(ps/r_0)\mathbf{r}(s/r_0) && (17)\\
\mathbf{D}^2(s) &= -\sin(ps/r_0)\mathbf{E}(s) + \cos(ps/r_0)\mathbf{r}(s/r_0) && (18)
\end{aligned}$$

where β is a constant (to be determined below), and p is the integer which determines the density of twist uniformly distributed along the rod. The reason we restrict p to integer values is so that

the triad will be continuous at $s = 0$, which is the same point as $s = 2\pi r_0$. For an axially symmetric rod, there is no physical discontinuity if we choose non-integer p, but this case needs to be handled with a triad that is not single-valued, and we avoid that situation here. The vector $\mathbf{D}^3$ lies on the tangent plane spanned with azimuthal and axial component but slightly tilted away from the tangent vector to the rod $\mathbf{X}(s)$. The vector $\mathbf{E}(s)$ is a useful reference vector orthogonal to $\mathbf{D}^3$ within the plane spanned by $\boldsymbol{\theta}$ and $\mathbf{z}$.

For simplicity, we consider an isotropic rod in this paper, i.e., $a_1 = a_2 \equiv a$, and we also assume that $b_1 = b_2 = b_3 \equiv b$.

By substituting the above formulae for $\mathbf{X}(s)$, $\mathbf{D}^1(s)$, $\mathbf{D}^2(s)$, and $\mathbf{D}^3(s)$ into the constitutive relations, (7) and (8), we can find formulae for $\mathbf{F}(s)$ and $\mathbf{N}(s)$. These results in turn can be substituted into the equilibrium equations (1-2) in the absence of any applied forces or moments, i.e., with $\mathbf{f}(s)$ and $\mathbf{n}(s)$ both equal to zero. It turns out that the two equilibrium equations are satisfied if and only if

$$r_1 = r_0 \cos\beta \tag{19}$$

$$\sin\beta = -\frac{a_3 p}{b r_0^2 + a_3 - a} \tag{20}$$

For large b, β is a small angle, which implies that the triad constructed above is nearly aligned with the rod, and also that r_1 is just slightly smaller than the unstressed radius r_0. In the limit $b \to \infty$, we recover the standard circular equilibrium of a twisted Kirchhoff rod. (See Figure 1.)

The behavior of $\mathbf{F}(s)$ in the solution constructed above, and indeed in the standard circular equilibrium of a twisted Kirchhoff rod, is perhaps somewhat unexpected, and we comment on it here. The first equilibrium equation states that $\mathbf{F}(s)$ has to be constant, independent of s, and one might then be tempted to conclude that $\mathbf{F}$ has to be zero, by symmetry. This conclusion is incorrect. What we actually find is

$$\mathbf{F} = -b(\sin\beta)\mathbf{z} \tag{21}$$

$$= \frac{b a_3 p}{b r_0^2 + a_3 - a}\mathbf{z} \tag{22}$$

As $b \to \infty$, $\mathbf{F} \to (a_3 p / r_0^2)\mathbf{z}$. Thus, the constant vector $\mathbf{F}$, which represents the force transmitted across a section of the rod, points normal to the horizontal plane in which the rod lies. This seems strange (what determines whether the force is up or down?) until we recall that $\mathbf{F}(s_0)$ is the force applied by the part of the rod for which s is slightly greater than s_0 to the part of the rod for which s is slightly less than s_0 across the section of the rod at $s = s_0$. A force of the same magnitude but pointing in the opposite direction is applied by the part of the rod with s slightly less than s_0 to the part with s slightly greater than s_0, so it is merely the direction in which we choose to traverse the rod that determines whether $\mathbf{F}$ points up or down. Nevertheless, this result is sufficiently peculiar that it leads Love [21], page 417, to state erroneously, "... and the shearing force at any section is directed towards the center of the circle..." This sounds reasonable, considering the symmetry of the problem, but it clearly cannot be correct, as it violates the equilibrium condition that $\mathbf{F}$ must be constant!

In computer simulations, however, we use a perturbed configuration as an initial configuration to see whether the equilibrium configuration constructed above is stable or unstable. A sinusoidal

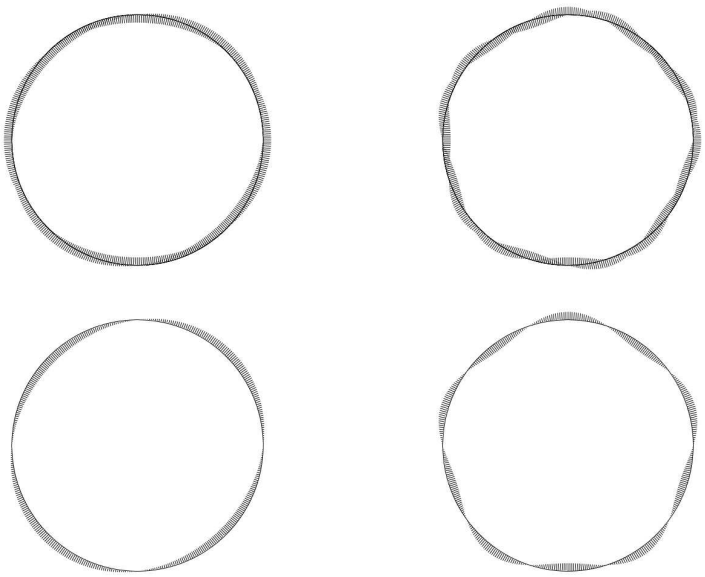

(a) *p*=2 (b) *p*=5

Figure 1: Examples of equilibrium configurations of a closed twisted circular rod, with p as the number of twists. Top row: with all vectors $\{\mathbf{D}^1, \mathbf{D}^2, \mathbf{D}^3\}$ of the triad shown. Bottom row: with only $\mathbf{D}^1$ shown.

perturbation can be obtained by making the following substitutions in the formulae for $\mathbf{D}^1$ and $\mathbf{D}^2$:

$$\sin(\frac{ps}{r_0}) \to \sin(\frac{ps}{r_0} + \epsilon \sin\frac{s}{r_0}) \tag{23}$$

$$\cos(\frac{ps}{r_0}) \to \cos(\frac{ps}{r_0} + \epsilon \sin\frac{s}{r_0}) \tag{24}$$

$$\tag{25}$$

where ϵ is a perturbation parameter (see Figure 2).

3 Mathematical formulation

The equations of motion for a bent, twisted rod immersed in a viscous incompressible fluid are stated in this section. They involve both Eulerian and Lagrangian variables. The Eulerian variables are used to describe the fluid, and the Lagrangian variables are used to describe the immersed rod. These two types of variables may be interconverted by means of integral transformations that involve a smoothed version of the three-dimensional Dirac delta function, as will be seen below.

We consider a viscous, incompressible fluid governed by the Navier-Stokes equations, and a closed bent and twisted rod immersed in that fluid. The immersed rod is represented as a one-dimensional closed curve with an associated orthonormal triad at each point of the curve. In

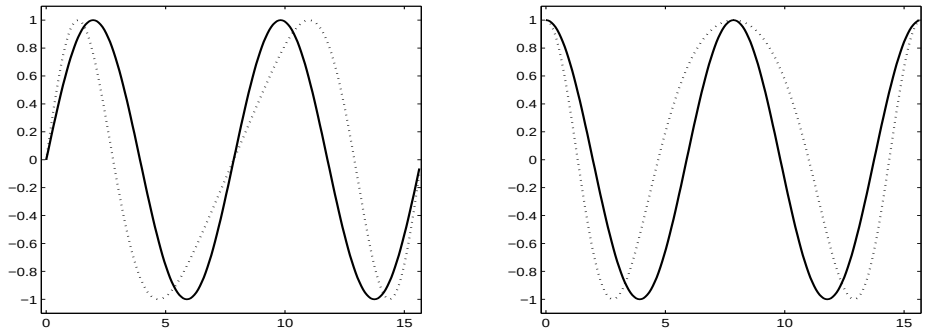

(a) (b)

Figure 2: Sinusoidal perturbation in $\{\mathbf{D}^1, \mathbf{D}^2\}$ when $p = 2, \epsilon = 1$. (a) sine function (solid) and its perturbation (dotted) (see Eq. (23)). (b) cosine function (solid) and its perturbation (dotted) (see Eq. (24)).

describing the immersed rod, we use the same notation as in the previous section. There, $\mathbf{f}(s)ds$ was the force applied by some unspecified external agent to the arc ds of the rod. Here, that external agent is the fluid, and therefore (according to Newton) $-\mathbf{f}(s)ds$ is the force applied by the arc ds of the rod to the fluid. Similarly $-\mathbf{n}(s)ds$ is the torque applied by the arc ds of the rod to the fluid.

The interaction of a viscous incompressible fluid with a thin elastic rod presents the following conceptual difficulty: On the one hand, it seems natural to represent the rod as a space curve (with its associated triad) as in the previous section. On the other hand, it is impossible to describe the interaction of a space curve with a three-dimensional fluid, since the application of a finite force per unit length along a curve in such a fluid results in a velocity field that is infinite on that curve. (This is in sharp contrast to the case of a surface, on which the application of finite force per unit area results in a finite velocity everywhere, including on the surface itself. The difference between these two cases is that the surface is co-dimension 1, whereas the curve is co-dimension 2.) Thus, we must somehow assign a cross-sectional radius to the space curve that represents the bent, twisted rod. In the present work, this will be done by replacing the Dirac delta function that appears in the interaction equations of the immersed boundary method by a smoothed approximation to the delta function that we denote δ_c where the subscript c denotes the order of magnitude of the support of the smoothed delta function. The specific form of δ_c will be specified below. In typical applications of the immersed boundary method, the mathematical formulation of the problem involves the true Dirac delta function, and a smoothed approximation to the delta function makes its appearance only at the level of the spatially discretized equations. Here, we need the smoothed approximation from the outset for our formulation to make sense, and it is important to keep in mind that c is a physical parameter of the problem, as it determines the effective radius of the rod. In practice, we choose the meshwidth h of the lattice on which the Navier-Stokes equations are solved equal to c in most of our simulations, but we also set it equal to $c/2$ for comparison, in order to check the convergence of our scheme. This convergence test is described at the end of the Results section.

Related to the above is the conceptual issue of the mass of the rod. We assume in the present work that the rod is neutrally buoyant, i.e., that its mass is equal to the mass of the fluid displaced. In an immersed boundary computation, however, the fluid is not displaced; it permeates the volume of radius $O(c)$ that surrounds the space curve that represents the rod. Thus, in our computational method, the fluid supplies the mass that is physically attributable to the rod, and the consistent way to model the space curve (with its associated triad) that represents the elasticity of the rod is as though it were massless. Since a massless structure is always at equilibrium, we may use unchanged the force balance equations of the previous section to describe the elastic component of our model system.

The coupled system of equations of the rod and the fluid is as follows:

$$\rho\left(\frac{\partial \mathbf{u}}{\partial t} + \mathbf{u}\cdot\nabla\mathbf{u}\right) = -\nabla p + \mu\nabla^2\mathbf{u} + \mathbf{f}^b \tag{26}$$

$$\nabla\cdot\mathbf{u} = 0 \tag{27}$$

$$0 = \mathbf{f} + \frac{\partial \mathbf{F}}{\partial s} \tag{28}$$

$$0 = \mathbf{n} + \frac{\partial \mathbf{N}}{\partial s} + \frac{\partial \mathbf{X}}{\partial s}\times\mathbf{F} \tag{29}$$

$$\mathbf{F} = F^1\mathbf{D}^1 + F^2\mathbf{D}^2 + F^3\mathbf{D}^3 \tag{30}$$

$$\mathbf{N} = N^1\mathbf{D}^1 + N^2\mathbf{D}^2 + N^3\mathbf{D}^3 \tag{31}$$

$$N^1 = a_1\frac{\partial \mathbf{D}^2}{\partial s}\cdot\mathbf{D}^3, \quad N^2 = a_2\frac{\partial \mathbf{D}^3}{\partial s}\cdot\mathbf{D}^1, \quad N^3 = a_3\frac{\partial \mathbf{D}^1}{\partial s}\cdot\mathbf{D}^2 \tag{32}$$

$$F^1 = b_1\mathbf{D}^1\cdot\frac{\partial \mathbf{X}}{\partial s}, \quad F^2 = b_2\mathbf{D}^2\cdot\frac{\partial \mathbf{X}}{\partial s}, \quad F^3 = b_3(\mathbf{D}^3\cdot\frac{\partial \mathbf{X}}{\partial s} - 1) \tag{33}$$

$$\mathbf{f}^b(\mathbf{x},t) = \int(-\mathbf{f}(s,t))\,\delta_c(\mathbf{x}-\mathbf{X}(s,t))ds + \frac{1}{2}\nabla\times\int(-\mathbf{n}(s,t))\delta_c(\mathbf{x}-\mathbf{X}(s,t))ds \tag{34}$$

$$\frac{\partial \mathbf{X}(s,t)}{\partial t} = \mathbf{U}(s,t) = \int\mathbf{u}(\mathbf{x},t)\,\delta_c(\mathbf{x}-\mathbf{X}(s,t))d\mathbf{x} \tag{35}$$

$$\mathbf{W}(s,t) = \frac{1}{2}\int(\nabla\times\mathbf{u})\delta_c(\mathbf{x}-\mathbf{X}(s,t))d\mathbf{x} \tag{36}$$

$$\frac{\partial \mathbf{D}^i(s,t)}{\partial t} = \mathbf{W}(s,t)\times\mathbf{D}^i(s,t), \quad i=1,2,3. \tag{37}$$

Equations (26-27) are the incompressible Navier-Stokes equations written in Eulerian variables $(\mathbf{x},t)$, where $\mathbf{x}=(x_1,x_2,x_3)$ are fixed Cartesian coordinates and t is the time. The motion of the fluid is subject to the body force $\mathbf{f}^{\mathrm{b}}(\mathbf{x},t)$, which here represents the force per unit volume applied to the fluid by the immersed rod. The vector field $\mathbf{u}(\mathbf{x},t)$ is the fluid velocity and $p(\mathbf{x},t)$ is the fluid pressure. The constant parameters ρ and μ are the fluid density and the fluid viscosity, respectively.

The equilibrium equations of the previous section (28-33) are employed to describe the force and torque of the immersed rod in terms of the space curve and its associated triad

$$\left(\mathbf{X}(s,t), \mathbf{D}^1(s,t), \mathbf{D}^2(s,t), \mathbf{D}^3(s,t)\right). \tag{38}$$

All variables in these equilibrium equations are functions of the material coordinate s (not necessarily arclength) and the time t. These are therefore Lagrangian variables. As in the previous section, $\mathbf{F}(s,t)$ and $\mathbf{N}(s,t)$ are the force and moment (couple) transmitted across the section of the rod at s. The expressions $-\mathbf{f}(s,t)ds$ and $-\mathbf{n}(s,t)ds$ are the force and torque applied by the arc ds of the rod to the fluid.

Equations (34-36) describe the interactions between the fluid and the rod. These interaction equations connect the Lagrangian and Eulerian variables via a three-dimensional smoothed Dirac delta function $\delta_c(\mathbf{x}) = \delta_c(x_1)\delta_c(x_2)\delta_c(x_3)$, which acts as a kernel of the integral transformations that appear in the interaction equations. The particular choice of $\delta_c(\mathbf{x})$ that we make in this work is the following:

$$\delta_c(\mathbf{x}) = \frac{1}{c^3}\phi(\frac{x_1}{c})\phi(\frac{x_2}{c})\phi(\frac{x_3}{c}) \tag{39}$$

where $\mathbf{x} = (x_1, x_2, x_3)$ and the function ϕ is given by

$$\phi(r) = \begin{cases} \dfrac{3 - 2|r| + \sqrt{1 + 4|r| - 4r^2}}{8} & \text{if } |r| \le 1, \\ \dfrac{5 - 2|r| - \sqrt{-7 + 12|r| - 4r^2}}{8} & \text{if } 1 \le |r| \le 2, \\ 0 & \text{if } |r| \ge 2. \end{cases}$$

The motivation for this particular construction is discussed in [28, 25]. Without going into all of the details, we note in particular that $\delta_c(\mathbf{x} - \mathbf{X})$ is a continuous function of $\mathbf{x}$ with continuous first derivatives and with support equal to a cube of edge $4c$ centered on $\mathbf{X}$. Whenever c is an integer multiple of h, the function $\delta_c(\mathbf{x} - \mathbf{X})$ satisfies two identities that are of particular importance in this work. Note in particular that these identities hold for all $\mathbf{X}$.

$$\sum_{\mathbf{j}} \delta_c(\mathbf{j}h - \mathbf{X})h^3 = 1 \tag{40}$$

$$\sum_{\mathbf{j}} (\mathbf{j}h - \mathbf{X})\delta_c(\mathbf{j}h - \mathbf{X})h^3 = 0 \tag{41}$$

where $\mathbf{j}$ is any vector with integer components, and h is the meshwidth of the fluid grid that will be introduced in the next section. As mentioned above, these identities hold only if c/h is a positive integer, and we shall choose h so that this is the case. The significance of the above identities will become apparent when we prove, in the next section, that force and torque generated by the rod are correctly applied to the fluid by our numerical scheme.

In equation (34), the first term describes how to apply the force of the rod to the fluid and the second term describes how to apply the torque of the rod to the fluid. To understand the meaning of equation (34), take the dot product of both sides with an arbitrary velocity field $\mathbf{u}(\mathbf{x}, t)$ and integrate by parts in the second term. (Note in particular that the overall sign of the second term

does not change upon this integration by parts because the usual sign change is compensated by a change of sign involving the antisymmetry of the cross product.) The result is

$$\int \mathbf{u}(\mathbf{x},t)\cdot\mathbf{f}^{\mathrm{b}}(\mathbf{x},t)d\mathbf{x} = \int(-\mathbf{f}(s,t))\cdot\mathbf{U}(s,t)ds + \int(-\mathbf{n}(s,t))\cdot\mathbf{W}(s,t)ds \qquad (42)$$

where $\mathbf{U}(s,t)$ is the locally averaged fluid velocity defined by equation (35) and $\mathbf{W}(s,t)$ is the locally averaged *angular* velocity of the fluid as defined by equation (36). Thus we have the result that the rate at which work is done on the fluid by the immersed rod is as it should be in terms of the force and moment applied to the fluid by the rod. Since this holds for an *arbitrary* velocity field, it establishes the validity of Eq. (34). Equation (35) is the no-slip condition of a viscous fluid, which means that the rod moves at the local fluid velocity. Here, the local fluid velocity is averaged in a manner determined by the smoothed Dirac delta function. Equation (36) states that angular velocity $\mathbf{W}(s,t)$ of the triad associated with the point s of the rod can be obtained as a local average of the angular velocity of the fluid, $\frac{1}{2}(\nabla\times\mathbf{u})$. Again, the smoothed delta function is used to determine the appropriate weighted average of the local fluid velocity.

We keep track of the orientation of the triad at each point of the rod by the equation (37). The triad rotates at the local angular velocity of the fluid, and applies torque locally to the fluid.

4 Numerical method

In this section, we describe the numerical IB method that we use to solve the equations of motion (26-37) as formulated in the preceding section.

The spatial discretization of the Eulerian (fluid) variables is different from that of the Lagrangian (rod) variables. For the fluid variables such as $\mathbf{u}$, p, and $\mathbf{f}^{\mathrm{b}}$, we use a fixed cubic lattice of mesh width h. This lattice, denoted g_h is the set of points, $g_h = \{\mathbf{x} : \mathbf{x} = \mathbf{j}h\}$, where $\mathbf{j} = (j_1, j_2, j_3) \in \mathbb{Z}^3$, i.e., a vector with integer components. Although our discretization makes sense on an infinite grid, in practice we use a lattice that is periodic in all three space directions. Thus $0 \le j_i \le N-1$, for $i = 1, 2, 3$, and it is understood that arithmetic involving any of the j_i is to be done modulo N. The periodicity facilitates the use of the discrete Fourier transform, and is less disruptive than other boundary conditions one might consider. In particular, a periodic domain (3-torus) is translation invariant, and all grid points are equivalent when periodic boundary conditions are used.

Spatial discretization of the immersed rod is accomplished by introducing a fixed uniform interval $\triangle s$ of the Lagrangian variable s of the rod, and then setting $s_k = k\triangle s$, for $k = 0, 1, ..., l-1$, where $l\triangle s$ is the unstressed length of the rod, and it is understood that all arithmetic on k is to be done modulo l, since the rod is in fact closed. For some variables, we shall consider half-integer as well as integer values of the index k. The Lagrangian variables $\mathbf{X}$, $\mathbf{D}^1$, $\mathbf{D}^2$, $\mathbf{D}^3$, $\mathbf{f}$, and $\mathbf{n}$ will all be defined at points s_k for integer values of k, and for such variables we shall use the notation $\mathbf{X}_k = \mathbf{X}(k\triangle s)$, etc. We shall need, however, to define auxiliary $\mathbf{D}^i$ at s_k for half-integer values of k, and the variables $\mathbf{F}$, and $\mathbf{N}$ will also be defined at s_k for half-integer values of k. For such variables, we shall write $\mathbf{D}^i_{k+\frac{1}{2}}$, etc., where k is again restricted to integer values.

Let the superscript n be the time-step index, so that $\mathbf{u}^n$ denotes the fluid velocity field at time $t = n\triangle t$, where $\triangle t$ is time step duration, and similarly for all other variables. We shall describe

here the step from time level n to $n+1$. To avoid cluttering the notation, however, we omit the time index in any equation where all of the variables are to be evaluated at time level n, i.e., at the beginning of the time step. This includes all of the equations involving the elasticity of the rod, which will be discussed first. The time index will make its appearance when we come to the fluid equations, and will continue to appear in the equations for updating the configuration of the rod.

The first thing that needs to be done in each time step is to compute the auxiliary triad at the point $s_{k+\frac{1}{2}}$ from the triads at s_k and s_{k+1}, where k is any integer. Intuitively, this is an interpolation process, but we cannot use anything like linear interpolation, since the result would not be an orthonormal triad. Therefore, we proceed as follows.

A rotation (orthogonal matrix) which maps from the triad $\mathbf{D}_k^\alpha$ to the triad $\mathbf{D}_{k+1}^\alpha$ ($\alpha = 1, 2, 3$) is uniquely defined by

$$A = \sum_{\alpha=1}^{3} \mathbf{D}_{k+1}^\alpha (\mathbf{D}_k^\alpha)^T \tag{43}$$

that is,

$$A = (a_{ij}) = \sum_{\alpha=1}^{3} (\mathbf{D}_{k+1}^\alpha)_i (\mathbf{D}_k^\alpha)_j \tag{44}$$

where ^{T} stands for the transpose of a matrix and $i, j = 1, 2, 3$; $k = 0, ..., l-1$.

This matrix A can be described as a rotation about a certain axis through a certain angle. To remove the ambiguity about the angle, we choose the one with smallest magnitude, which is also the one lying in the interval $(-\pi, \pi]$.

In order to find an orthonormal triad $\{\mathbf{D}_{k+\frac{1}{2}}^1, \mathbf{D}_{k+\frac{1}{2}}^2, \mathbf{D}_{k+\frac{1}{2}}^3\}$ for the point $s_{k+\frac{1}{2}}$ we can take the principal square root of the matrix A, which is a rotation about that same axis by half the angle (and make sure that half the angle should be in the interval $(-\pi/2, \pi/2]$), and apply this rotation to each vector of the triad at s_k, i.e.,

$$\mathbf{D}_{k+\frac{1}{2}}^i = \sqrt{A}\mathbf{D}_k^i \tag{45}$$

where $i = 1, 2, 3$. This will give the desired triad at $s_{k+\frac{1}{2}}$.

The next step is to evaluate the force $\mathbf{F}_{k+\frac{1}{2}}$ and the couple or moment $\mathbf{N}_{k+\frac{1}{2}}$ that are transmitted across the section of the rod at $s_{k+\frac{1}{2}}$. The computations are as follows. First evaluate the

components:

$$F^1_{k+\frac{1}{2}} = b_1 \mathbf{D}^1_{k+\frac{1}{2}} \cdot \frac{\mathbf{X}_{k+1} - \mathbf{X}_k}{\triangle s} \tag{46}$$

$$F^2_{k+\frac{1}{2}} = b_2 \mathbf{D}^2_{k+\frac{1}{2}} \cdot \frac{\mathbf{X}_{k+1} - \mathbf{X}_k}{\triangle s} \tag{47}$$

$$F^3_{k+\frac{1}{2}} = b_3 (\mathbf{D}^3_{k+\frac{1}{2}} \cdot \frac{\mathbf{X}_{k+1} - \mathbf{X}_k}{\triangle s} - 1) \tag{48}$$

$$N^1_{k+\frac{1}{2}} = a_1 \frac{\mathbf{D}^2_{k+1} - \mathbf{D}^2_k}{\triangle s} \cdot \mathbf{D}^3_{k+\frac{1}{2}} \tag{49}$$

$$N^2_{k+\frac{1}{2}} = a_2 \frac{\mathbf{D}^3_{k+1} - \mathbf{D}^3_k}{\triangle s} \cdot \mathbf{D}^1_{k+\frac{1}{2}} \tag{50}$$

$$N^3_{k+\frac{1}{2}} = a_3 \frac{\mathbf{D}^1_{k+1} - \mathbf{D}^1_k}{\triangle s} \cdot \mathbf{D}^2_{k+\frac{1}{2}} \tag{51}$$

which are discretizations of Eqs. (32-33), and then assemble the vectors:

$$\mathbf{F}_{k+\frac{1}{2}} = F^1_{k+\frac{1}{2}} \mathbf{D}^1_{k+\frac{1}{2}} + F^2_{k+\frac{1}{2}} \mathbf{D}^2_{k+\frac{1}{2}} + F^3_{k+\frac{1}{2}} \mathbf{D}^3_{k+\frac{1}{2}} \tag{52}$$

$$\mathbf{N}_{k+\frac{1}{2}} = N^1_{k+\frac{1}{2}} \mathbf{D}^1_{k+\frac{1}{2}} + N^2_{k+\frac{1}{2}} \mathbf{D}^2_{k+\frac{1}{2}} + N^3_{k+\frac{1}{2}} \mathbf{D}^3_{k+\frac{1}{2}}. \tag{53}$$

What this last step means operationally is to evaluate the *Cartesian* components of these vectors. This is very important for what follows, since we want to compare these vectors at different locations, see below, and this cannot be done merely by comparing their components in the basis given by the moving triad.

With $\mathbf{F}_{k+\frac{1}{2}}$ and $\mathbf{N}_{k+\frac{1}{2}}$ known for all k, we can proceed to the computation of $-\mathbf{f}_k$ and $-\mathbf{n}_k$ by the following discretization of Eqs. 1-2. These quantities, multiplied in each case by ds, give the force and torque applied to the fluid by the segment of the rod corresponding to the interval ds centered on s_k.

$$-\mathbf{f}_k = \frac{\mathbf{F}_{k+\frac{1}{2}} - \mathbf{F}_{k-\frac{1}{2}}}{\triangle s} \tag{54}$$

$$-\mathbf{n}_k = \frac{\mathbf{N}_{k+\frac{1}{2}} - \mathbf{N}_{k-\frac{1}{2}}}{\triangle s} + \frac{1}{2}\left(\frac{\mathbf{X}_{k+1} - \mathbf{X}_k}{\triangle s} \times \mathbf{F}_{k+\frac{1}{2}} + \frac{\mathbf{X}_k - \mathbf{X}_{k-1}}{\triangle s} \times \mathbf{F}_{k-\frac{1}{2}} \right). \tag{55}$$

This completes the purely Lagrangian part of the computation during any one time step.

The force and torque generated by the elasticity of the rod can now be applied to the fluid by creating the body force $\mathbf{f}^{\mathrm{b}}$ on the fluid grid defined as follows:

$$\mathbf{f}^{\mathrm{b}}(\mathbf{x}) = \sum_k (-\mathbf{f}_k)\, \delta_c(\mathbf{x} - \mathbf{X}_k) \triangle s + \frac{1}{2}\mathbf{G}^0 \times (\sum_k (-\mathbf{n}_k)\, \delta_c(\mathbf{x} - \mathbf{X}_k) \triangle s) \tag{56}$$

where $\mathbf{x} \in g_h$, and δ_c has been defined in the preceding section. Recall in particular the restriction that c/h must be a positive integer.

Here, and throughout the paper, $\mathbf{G}^0$ denotes the central-difference approximation to ∇ defined on the Eulerian grid g_h by $\mathbf{G}^0 = (G_1^0, G_2^0, G_3^0)$, where G_α^0, is the standard central difference operator in the spatial direction $\alpha = 1, 2, 3$ defined by

$$\left(G_\alpha^0 \psi\right)(\mathbf{x}) = \frac{\psi(\mathbf{x} + h\mathbf{e}^\alpha) - \psi(\mathbf{x} - h\mathbf{e}^\alpha)}{2h} \tag{57}$$

where $\{\mathbf{e}^1, \mathbf{e}^2, \mathbf{e}^3\}$ is a fixed orthonormal basis that specifies the orientation of the Cartesian lattice on which the Eulerian variables of our fluid mechanics computation are defined. In the following we shall also make use of the forward and backward difference operators in each of the three spatial directions $\alpha = 1, 2, 3$. These are defined by

$$\left(G_\alpha^+ \psi\right)(\mathbf{x}) = \frac{\psi(\mathbf{x} + h\mathbf{e}^\alpha) - \psi(\mathbf{x})}{h} \tag{58}$$

$$\left(G_\alpha^- \psi\right)(\mathbf{x}) = \frac{\psi(\mathbf{x}) - \psi(\mathbf{x} - h\mathbf{e}^\alpha)}{h}. \tag{59}$$

Up to this point, all quantities have been defined at time level n, i.e., at the beginning of the time step, and the superscript n indicating the time level has been omitted. Here, we begin to describe the computation of variables defined at time level $n+1$ from those at time level n, so we include the superscript that indicates the time level from now on.

With $\mathbf{u}^n$ and $(\mathbf{f}^{\mathrm{b}})^n$ known, we solve the discretized Navier-Stokes equations for the unknowns $(\mathbf{u}^{n+1}, p^{n+1})$:

$$\rho\left(\frac{\mathbf{u}^{n+1} - \mathbf{u}^n}{\triangle t} + \sum_{\alpha=1}^{3} u_\alpha^n G_\alpha^{\pm} \mathbf{u}^n\right) + \mathbf{G}^0 p^{n+1} = \mu \sum_{\alpha=1}^{3} G_\alpha^+ G_\alpha^- \mathbf{u}^{n+1} + (\mathbf{f}^{\mathrm{b}})^n \tag{60}$$

$$\mathbf{G}^0 \cdot \mathbf{u}^{n+1} = 0. \tag{61}$$

In these equations, the operator $\mathbf{G}^0 p$ approximates ∇p, and $\mathbf{G}^0 \cdot \mathbf{u}$ approximates $\nabla \cdot \mathbf{u}$. In the viscous term, the expression $\sum_{\alpha=1}^{3} G_\alpha^+ G_\alpha^-$ is a difference approximation to the Laplace operator. In the convection term, the expression $\sum_{\alpha=1}^{3} u_\alpha G_\alpha^{\pm}$, where

$$u_\alpha G_\alpha^{\pm} = \begin{cases} u_\alpha G_\alpha^+, & u_\alpha < 0, \\ u_\alpha G_\alpha^-, & u_\alpha > 0, \end{cases}$$

is an upwind difference approximation to $\mathbf{u} \cdot \nabla$. We use the FFT (fast Fourier transform) to solve the system of equations (60-61). Note that this system is linear with constant coefficients in the unknowns $(\mathbf{u}^{n+1}, p^{n+1})$, the nonlinear terms being known since they are evaluated at time level n. The FFT therefore uncouples this system into N^3 separate 4×4 systems, which are easily solved.

Once $\mathbf{u}^{n+1}$ is known, the boundary points are moved at the locally averaged fluid velocity in this new velocity field. This is done as follows:

$$\frac{\mathbf{X}_k^{n+1} - \mathbf{X}_k^n}{\triangle t} = \sum_{\mathbf{x}} \mathbf{u}^{n+1}(\mathbf{x}) \delta_c(\mathbf{x} - \mathbf{X}_k^n) h^3 \tag{62}$$

where $\sum_{\mathbf{x}}$ denotes the sum over the computational lattice $\mathbf{x} \in g_h$.

The last step of the numerical procedure is to update the orientation of the triad at each point s_k of the rod. Each such triad rotates at the local angular velocity of the fluid. Recall that the local angular velocity of a fluid element is $\frac{1}{2}\nabla \times \mathbf{u}$. We discretize this as $\frac{1}{2}\mathbf{G}^0 \times \mathbf{u}$, and compute its local average at the point s_k of the rod as follows:

$$\mathbf{W}_k^{n+1} = \frac{1}{2}\sum_{\mathbf{x}\in g_h} (\mathbf{G}^0 \times \mathbf{u}^{n+1})(\mathbf{x})\delta_c(\mathbf{x} - \mathbf{X}_k^n)h^3. \tag{63}$$

Now let $R(\mathbf{e}, \theta)$ be the orthogonal matrix that describes a rotation through an angle θ about the axis specified by the unit vector $\mathbf{e}$. We can write R explicitly as follows:

$$R(\mathbf{e}, \theta) = (\cos\theta)I + (1 - \cos\theta)\mathbf{e}\mathbf{e}^T + (\sin\theta)(\mathbf{e}\times) \tag{64}$$

where $(\mathbf{e}\times)$ is the antisymmetric 3×3 matrix defined by $(\mathbf{e}\times)\mathbf{v} = \mathbf{e}\times\mathbf{v}$, for any $\mathbf{v}$. We emphasize that $\mathbf{e}$ is a unit vector. In terms of R, the rotation that we need to apply to the triad located at point s_k of the rod is given by

$$(\mathbf{D}_k^i)^{n+1} = R\left(\frac{\mathbf{W}_k^{n+1}}{|\mathbf{W}_k^{n+1}|}, |\mathbf{W}_k^{n+1}|\triangle t\right)(\mathbf{D}_k^i)^n \tag{65}$$

where $i = 1, 2, 3$ and $k = 0, ..., l-1$. Thus, we rotate each triad at the locally averaged angular velocity of the fluid for an amount of time equal to $\triangle t$, and this completes the time step.

Note that the above rotation is free in the sense that we do not constrain the vector $\mathbf{D}^3$ to be tangent to the curve that describes the axis of the rod. Insofar as $\mathbf{D}^3$ deviates from that direction, however, forces are called into play that tend to correct the misalignment. A similar remark may be made concerning the update of the position $\mathbf{X}(s)$. There is nothing in the updating procedure that constrains s to be arclength. Insofar as s deviates from arclength, however, forces develop that tend to correct for those deviations.

We conclude this section with a proof that the body force $\mathbf{f}^{\mathrm{b}}$ defined by Eq. (56) applies the correct total force and also the correct total torque to the fluid. To avoid complications associated with the definition of torque on a periodic domain, we imagine here the fluid domain is the whole three-dimensional Euclidean space and that g_h is an unbounded computational lattice. Since the rod is described by a continuous closed curve it lives at any given time within a bounded subset of this domain. Because δ_c has bounded support, it is then clear that $\mathbf{f}^{\mathrm{b}}$ has bounded support as well. Thus, all of the sums that appear in the proof have only a finite number of nonzero terms, so there are no issues of convergence, and we do not have to worry about boundary terms when we do summation by parts. The proof given here relies in an essential way on the identities stated in the previous section for δ_c, Eqs. (40-41), and the proof therefore requires the assumption that c/h is a positive integer.

First consider the total force applied by the rod to the fluid. We sum Eq. (56) over g_h and multiply by h^3. Now it is easy to see that

$$\sum_{\mathbf{x}\in g_h} (\mathbf{G}^0 \times \mathbf{v})(\mathbf{x})h^3 = 0 \tag{66}$$

for any $\mathbf{v}(\mathbf{x})$ with bounded support, so the second term in $\mathbf{f}^{\mathrm{b}}$ makes no contribution. We are left with

$$\sum_{\mathbf{x}\in g_h} \mathbf{f}^{\mathrm{b}}(\mathbf{x})h^3 = \sum_{k=0}^{l-1}(-\mathbf{f}_k) \sum_{\mathbf{x}\in g_h} \delta_c(\mathbf{x}-\mathbf{X}_k)h^3\triangle s = \sum_{k=0}^{l-1}(-\mathbf{f}_k)\triangle s \tag{67}$$

In the first step, we have interchanged the order to the two summations, and in the second step we have made use of Eq. (40).

Next we consider the more complicated case of the total torque. This time we apply the operator $\mathbf{x}\times$ to both sides of Eq. (56) before summing over $\mathbf{x} \in g_h$ and multiplying by h^3. We consider the two terms on the right-hand side separately. In analyzing the first term it is helpful to note that the two identities Eqs. (40) and (41) can be combined to yield

$$\sum_{\mathbf{x}\in g_h} \mathbf{x}\delta_c(\mathbf{x}-\mathbf{X})h^3 = \mathbf{X} \tag{68}$$

Making use of this result, we see that

$$\begin{aligned}\sum_{\mathbf{x}\in g_h} \mathbf{x}\times\sum_{k=0}^{l-1}(-\mathbf{f}_k)\delta_c(\mathbf{x}-\mathbf{X}_k)\triangle s h^3 &= \sum_{k=0}^{l-1}\left(\sum_{\mathbf{x}\in g_h}\mathbf{x}\delta_c(\mathbf{x}-\mathbf{X}_k)h^3\right)\times(-\mathbf{f}_k)\triangle s \\ &= \sum_{k=0}^{l-1}\mathbf{X}_k\times(-\mathbf{f}_k)\triangle s \end{aligned}\tag{69}$$

In the case of the second term, it is helpful to work in components. The α component of the second term is

$$\frac{1}{2}\epsilon_{\alpha\beta\gamma}\epsilon_{\gamma\lambda\mu}\sum_{\mathbf{x}\in g_h} x^\beta G^0_\lambda \sum_{k=0}^{l-1}(-n_k^\mu)\delta_c(\mathbf{x}-\mathbf{X}_k)\triangle s h^3 \tag{70}$$

where we employ the summation convention and the totally antisymmetric symbol ϵ. This expression can be simplified by making use of summation by parts, in which we change the sign and apply G^0_λ to x^β instead of the expression on its right. It is easy to see that $G^0_\lambda x^\beta = \delta_{\lambda\beta}$. Now

$$\epsilon_{\alpha\beta\gamma}\epsilon_{\gamma\lambda\mu}\delta_{\beta\lambda} = (\delta_{\alpha\lambda}\delta_{\beta\mu}-\delta_{\alpha\mu}\delta_{\beta\lambda})\delta_{\beta\lambda} = (1-3)\delta_{\alpha\mu} = -2\delta_{\alpha\mu} \tag{71}$$

It follows, with the help of the identity given by Eq. (40) that the expression given by (70) reduces all the way down to

$$\sum_{k=0}^{l-1}(-n_k^\alpha)\triangle s \tag{72}$$

Combining this with the result for the first term, Eq. (69), we see that

$$\sum_{\mathbf{x}\in g_h}\mathbf{x}\times\mathbf{f}^{\mathrm{b}} = \sum_{k=0}^{l-1}\left((\mathbf{X}_k\times(-\mathbf{f}_k))+(-\mathbf{n}_k)\right)\triangle s \tag{73}$$

Equations (67) and (73) show that our numerical algorithm does indeed apply the correct total force and the correct total torque to the fluid. These equations therefore imply that neither

Table 1: Computational parameters.

Computational domain (cubic)	$10\,\mathrm{cm} \times 10\,\mathrm{cm} \times 10\,\mathrm{cm}$
Fluid grid	$64 \times 64 \times 64$
Meshwidth for fluid, h	$0.1562\,\mathrm{cm}$
Fluid density, ρ	$1\mathrm{g/cm}^3$
Fluid viscosity, μ	$0.01\mathrm{g/cm} \cdot \mathrm{s}$
Radius of the unstressed rod, r_0	$2.5\,\mathrm{cm}$
Number of boundary points, n	200
Meshwidth for rod, $\triangle s$	$0.0785\,\mathrm{cm}$
Time step, $\triangle t$	$0.01\,\mathrm{sec}$

momentum nor angular momentum is spuriously created or destroyed in the rod-fluid interaction step of our computational scheme.

Because Eqs. (67) and (73) are identities that hold for *any* distribution of force and torque applied by the rod to the fluid, and because the forces and torques are clearly applied *locally* on account of the bounded support of δ_c, the significance of these results is greater than it may at first appear. It is not merely a question of the *total* force and torque being correct, but also that the force and torque applied by any *part* of the rod are correctly transmitted to the fluid. This follows from the above by decomposing the force and torque into parts (e.g., by using a partition of unity along the rod), and then applying the above identities to each part separately.

5 Results and discussion

In this section, we study the evolution in time of a closed twisted rod immersed in a viscous incompressible fluid. The rod starts out in a configuration which is a perturbation of the circular equilibrium derived above (Section 2). Depending on parameters, the perturbation may decay, in which case the rod relaxes to the circular equilibrium configuration, or it may grow, in which case the rod and the surrounding fluid undergo a large-amplitude motion that eventually leads the rod into a stable coiled configuration in which self-contact of the rod plays an important role.

The computational and physical parameters that we regard as standard are summarized in Table 1 and Table 2. Deviations from these values will be explicitly stated where they occur. A particularly important parameter is the number of twists, p, which we choose as an integer for reasons that have been discussed above. When other parameters are held fixed, the circular equilibrium of the rod is stable for sufficiently small p and becomes unstable at some critical value of p. Also, in the unstable cases, the coiled configuration that the rod eventually finds depends on the value of p.

With these chosen parameters, we find that when $p = 0, 1, 2$, the circular equilibrium of the closed twisted rod is stable. When $p \geq 3$, the circular equilibrium is unstable, and the rod evolves into different coiled shapes that depend on p. In fact, as p increases, the number of loops in the final coiled configuration increases as well (see second column of snapshots in Figure 7).

Figure 3 shows motions at different instants when $p = 2$. The initial configuration in this case is a strong perturbation away from the circular equilibrium, since $\epsilon = 10$ (see Eqs. (23–24)).

Table 2: Material properties of the rod.

Bending modulus, $a_1 = a_2 = a$	$0.3\,\mathrm{dyne}\cdot\mathrm{cm}^2$
Twist modulus, a_3	$0.2\,\mathrm{dyne}\cdot\mathrm{cm}^2$
Shear force constant, $b_1 = b_2 = b$	$54\,\mathrm{dyne}$
Stretch force constant, $b_3 = b$	$54\,\mathrm{dyne}$
Number of twist, p	$0, 1, 2, 3, 4, 5, 6$

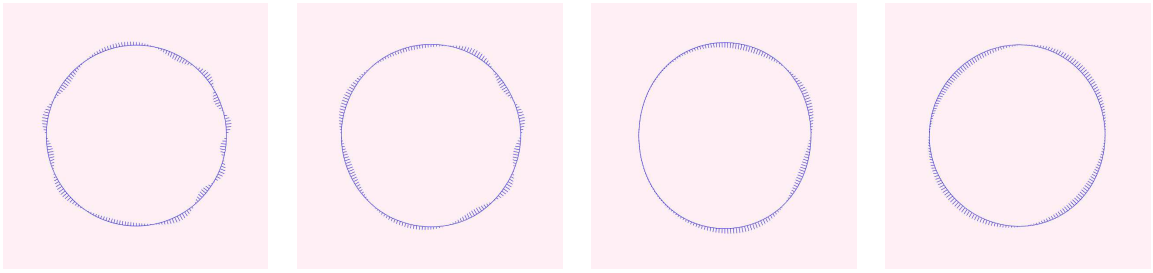

(a) $t = 0s$ (b) $t = 1.1s$ (c) $t = 2.5s$ (d) $t = 11s$

Figure 3: (a) Initial configuration with a rod (circle) and $\mathbf{D}^1$, (b)-(d) are snapshots at time t in seconds. Parameters: an intrinsic twist $p = 2$, elastic material properties $a = 0.3, a_3 = \frac{2}{3}a, b = 54$ in CGS unit, and perturbation parameter $\epsilon = 10$.

Despite the large initial perturbation, we see that the rod relaxes back to the circular equilibrium in this case. (Compare Figure 3 (d) and Figure 1 (a), lower frame.)

The writhing dynamics that emerge in cases $p = 4, 5, 7$, in which the circular equilibrium is unstable, are shown in figures 4-6. In all three cases, we start very close to the circular equilibrium configuration by setting $\epsilon = 0.001$. Each figure shows the rod and its associated triad in blue, and selected fluid markers that start out near the rod are shown in red. The fluid markers leave trails that show their recent trajectories. At each selected time, two different views of the rod and fluid markers are shown. The selected times are not equally spaced. Note in particular the long time that it takes the perturbation to grow to a significant size in comparison to the rapid evolution that happens thereafter. This is especially pronounced at the lower unstable values of p. Throughout the complicated motions shown in these figures, the rod retains its initial length to within 2%.

In Figure 4, the closed rod gradually takes on the configuration of a figure-eight structure (see frame (d)) and then the two loops of the figure-eight twist in opposite directions. The resulting coiled equilibrium is called a *plectoneme* [5, 13]. Note that the number of self-contact points increases with time as the rod approaches its coiled equilibrium.

Figure 5 shows the case in which the intrinsic twist is $p = 5$. The equilibrium configuration in Figure 5 (e) has three points of self-contact and three loops. Figure 6 with $p = 7$ shows an equilibrium *clover* configuration with four self-contact points.

In Figure 7, we vary the twist modulus in order to see what impact that has on the stability of the rod. The figure shows an array of results after the motion has settled down. Each row corresponds to a particular value of the intrinsic twist p, and each column corresponds to a particular

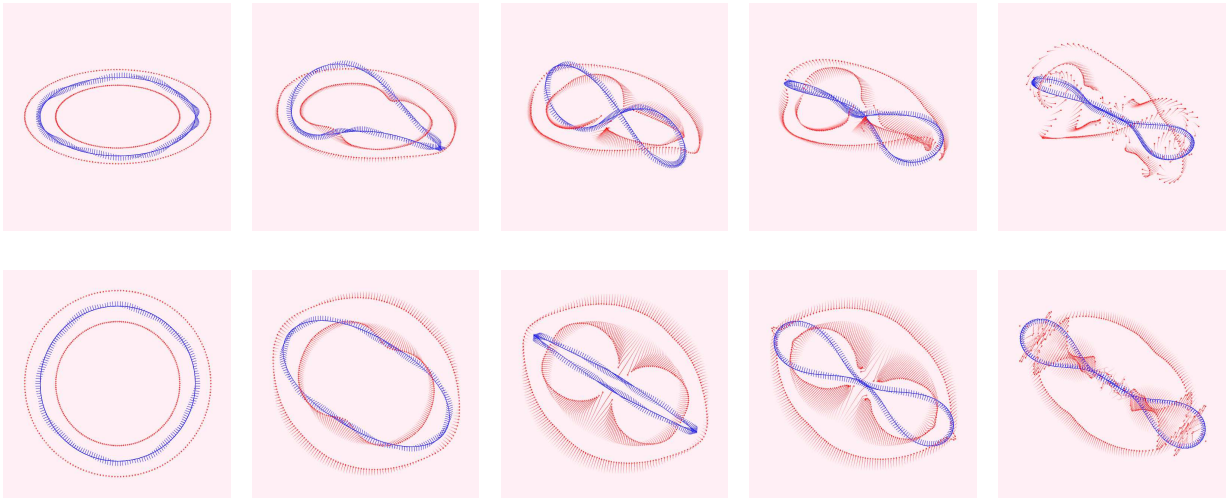

(a) $t = 0s$ (b) $t = 157.5s$ (c) $t = 163.5s$ (d) $t = 168s$ (e) $t = 183s$

Figure 4: Snapshots showing the rod and all vectors of the triads at each boundary point at time t. Top row and bottom row illustrate side views and top views of the motion, respectively. The number of twist is $p = 4$, and material properties are $a = 0.3, a_3 = \frac{2}{3}a, b = 54$, in CGS unit, and perturbation parameter is $\epsilon = 0.001$. Fluid markers in red are spread around the rod and show their trajectories.

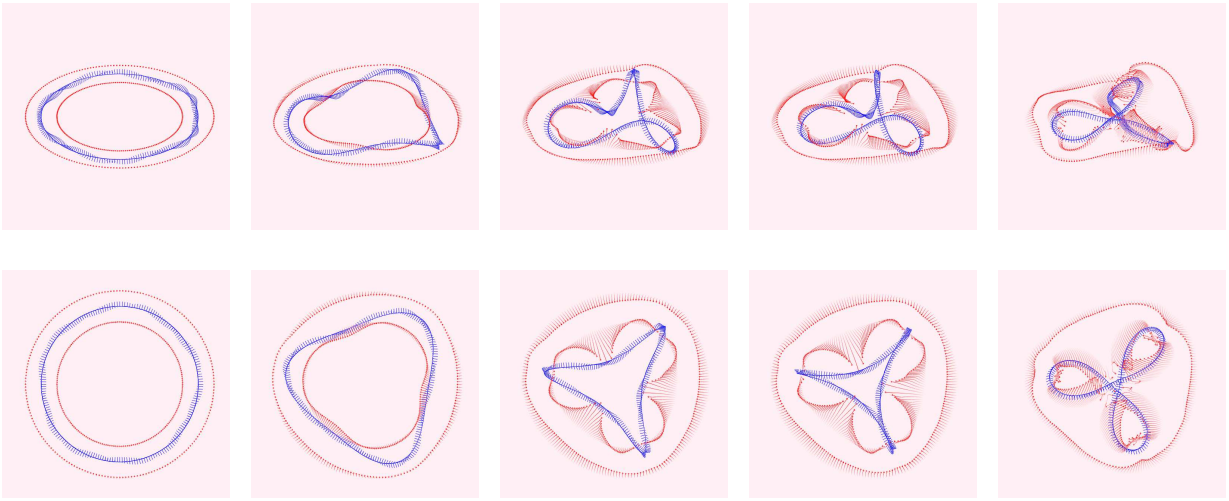

(a) $t = 0s$ (b) $t = 92s$ (c) $t = 97s$ (d) $t = 98s$ (e) $t = 105s$

Figure 5: Snapshots showing the rod and all vectors of the triads at each boundary point at time t together with fluid markers in red. Parameters: $p = 5$, $a = 0.3, a_3 = \frac{2}{3}a, b = 54$, and $\epsilon = 0.001$. First row is viewed from side and second row from top of the motion.

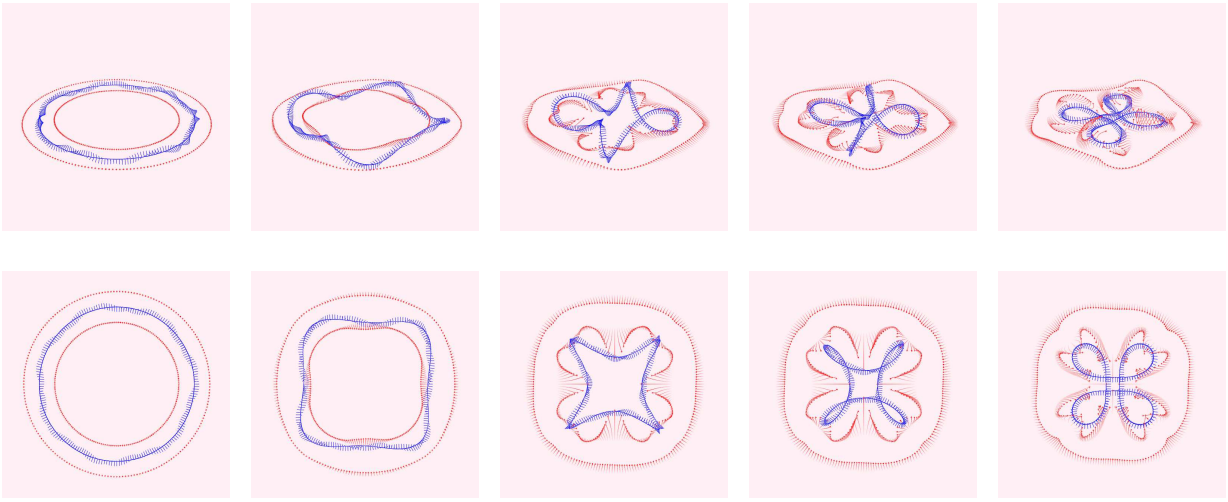

(a) $t = 0s$ (b) $t = 16s$ (c) $t = 19.5s$ (d) $t = 20.5s$ (e) $t = 23s$

Figure 6: Snapshots showing the rod and all vectors of the triads at each boundary point at time t together with fluid markers. Parameters: $p = 7$, $a = 0.3, a_3 = \frac{2}{3}a, b = 54$, and $\epsilon = 0.001$. First row is viewed from side and second row from top of the motion.

value of the twist modulus (reported in terms of the ratio of the twist modulus to the bend modulus, a_3/a). It is readily apparent from the figure that the stability boundary of the circular equilibrium configuration moves in the direction of lower intrinsic twist as the twist modulus increases. Another result of this study is that the number of loops formed during coiling increases both as a function of the intrinsic twist and also as a function of the twist modulus.

Note that the first and last columns of Figure 7 consider cases that cannot be achieved if the circular rod is made out of a homogeneous, isotropic elastic material with the whole cross section filled. We include these cases because the anisotropic microstructures that occur in biological settings make possible a wider range of ratios of the twist to the bend modulus.

When the circular equilibrium configuration is unstable, the coiled configuration that is eventually reached may depend on the initial condition. To study this, we compare results computed with all parameters held fixed other than ϵ, which measures the amplitude of the initial perturbation. Qualitatively different configurations of the rod appear, each associated with an interval of values of ϵ, as shown in Figure 8, which depicts a typical configuration for each such interval. In order of increasing ϵ, the configurations seen may be described as follows: (a) a three-leaf clover, (b) a configuration with two self-contact points, (c) a configuration with two well separated *sets* of closely spaces contact points, and (d) a plectoneme. According to [5], the clover and plectoneme configurations are stable, but the others are not. This suggests that further evolution would have been seen in the two intermediate cases if we had waited long enough for it to occur.

In many of the above examples, the rod comes to rest in a configuration that involves self-contact. We emphasize that this occurs without any special mechanism for detecting or responding to a self-contact condition. Even though further reduction of the elastic potential energy would result from the rod moving through itself in these situations, it does not do so. The reason is inherent in the immersed boundary method: The rod moves in the continuous velocity field of the

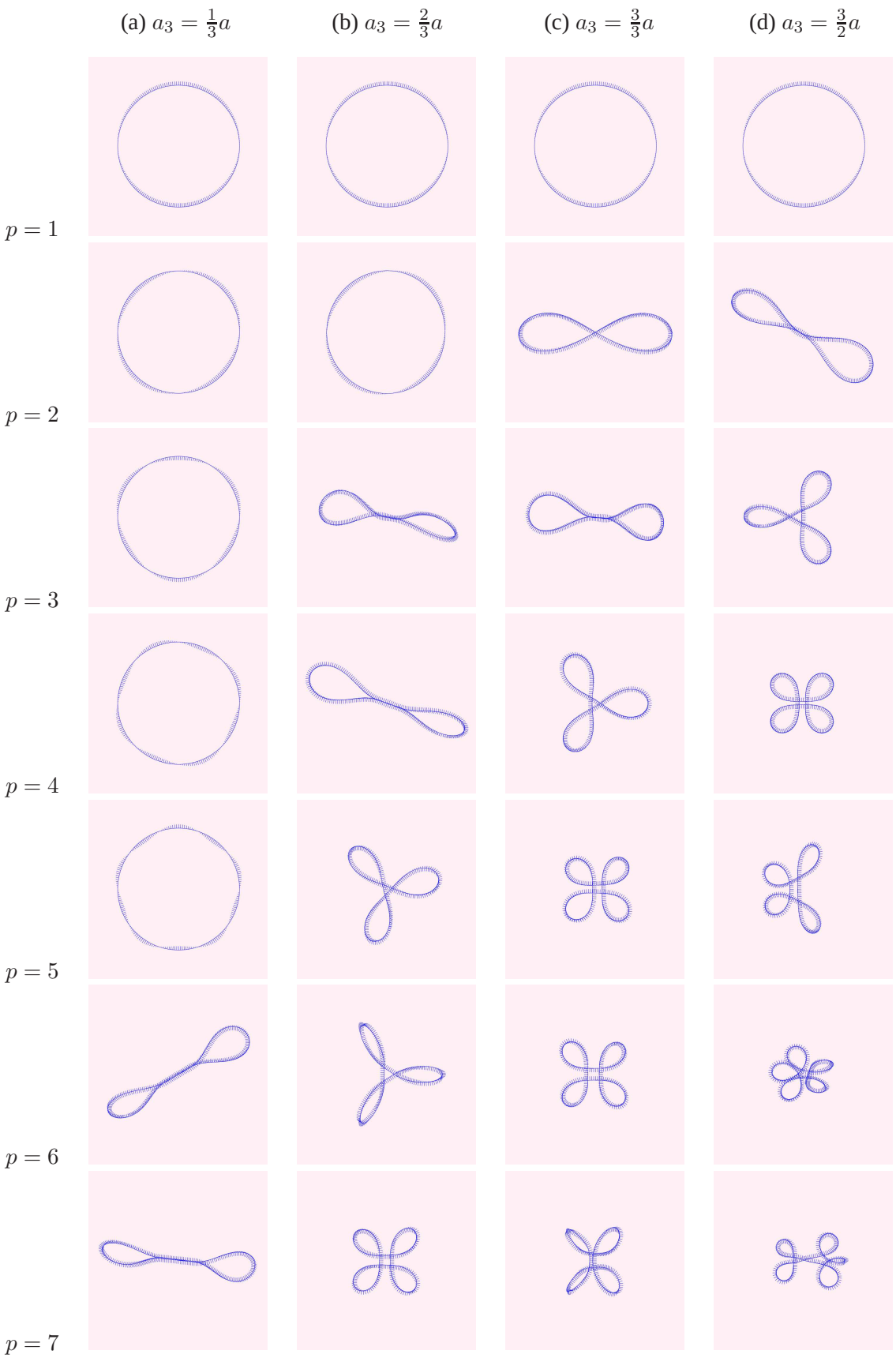

Figure 7: Collection of stable equilibria depending on ratio of $\frac{a_3}{a}$ and the initial twist p. Parameters: $a = 0.3, b = 54$ in CGS unit and $\epsilon = 0.001$.

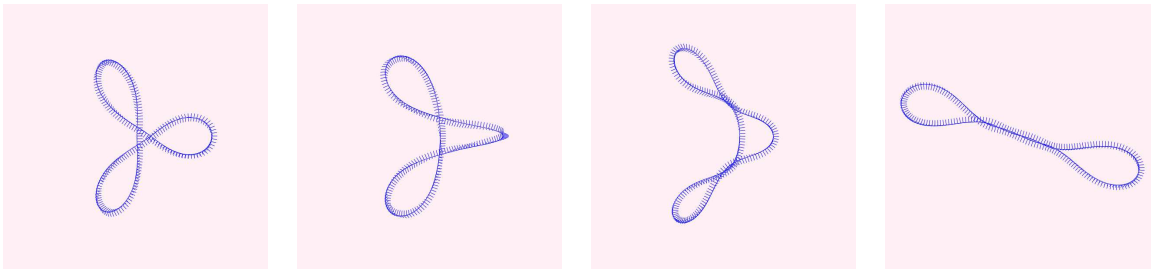

(a) $0 < \epsilon \leq 0.175$ (b) $0.2 \leq \epsilon \leq 0.275$ (c) $0.3 \leq \epsilon \leq 0.35$ (d) $\epsilon \geq 0.375$

Figure 8: Transition of configurations with the increments in perturbation parameter ϵ. All other parameters are fixed: $a = 0.3, a_3 = \frac{2}{3}a, b = 54$, and $p = 5$.

fluid. Therefore, at the level of the continuous formulation of the problem, self-crossing is impossible. Even after discretization, the immersed boundary points that represent the rod move in a continuous velocity field (with continuous first spatial derivatives) that is obtained by interpolation from the fluid grid. Nevertheless, self crossing of the rod in the discrete case is possible, for two reasons: the continuous rod has been replaced by a discrete array of points, and the motion occurs in discrete time steps instead of continuously. In practice, though, when the time step is small enough, and when the spacing between the immersed boundary points is small enough in relation to the resolution of the fluid grid, self-crossing does not occur.

It is both amusing and instructive to see what happens when the numerical parameters are not well chosen, and self-crossing does occur. First the immersed rod seems to settle into a coiled configuration with self-contact, like those shown above. It takes some time for self-crossing to occur, since the velocities of two immersed boundary points that are nearly in contact are nearly equal. Once self-crossing does occur, it reduces the number of twists in the rod, and this may change the stability of the circular equilibrium configuration from unstable to stable. In such a case, the rod that has crossed itself relaxes back to the circular configuration from which (except for a small perturbation) it started, although the final configuration is not really the same as the initial condition because of the reduction in the intrinsic twist that occurred during the topological transition in which the rod crossed itself.

It is not practical to do a full convergence study to determine the empirical order of accuracy of the method, since this requires at least three different meshwidths and the computational demands are too great. Instead we compare numerical solutions obtained on two different meshes, 64^3 (with 200 immersed boundary points representing the rod) and 128^3 (with 400 immersed boundary points representing the rod), at a given time, to check that the results are relatively insensitive to the mesh width. As we refine the computational mesh of the fluid grid, we follow the unusual procedure of keeping the *physical* size of the support of the delta function constant. When we change from a 64^3 grid to a 128^3 grid, this implies that the numerical support of the delta function grows from 4^3 to 8^3 points. In physical variables, we use the same delta function in both cases; in units of meshwidths the delta function for the refined mesh is obtained from the one for the coarse mesh by a simple scaling by a factor of two in each space direction. The rationale for this procedure is that the diameter of the support of the delta function is a physical rather than a numerical parameter in this work; it corresponds at least roughly to the diameter of the rod, since

it determines the size of the region of fluid with which any given point of the rod interacts directly, and therefore it should not be refined as the fluid grid is refined. (Recall that we represent the rod by an immersed space curve, together with an associated orthonormal triad at each point of that space curve. Such a curve, obviously, occupies zero volume, unlike the physical rod that we are trying to represent. There is, however, a nonzero volume of fluid within the support of the delta function, and this part of the fluid is the part that directly feels the force and torque generated by the rod, and also the part that directly determines the velocity with which the rod moves and the angular velocity with which its triads rotate. For these reasons, the volume of fluid within the support of the delta function in our immersed boundary formulation may be said to model the rod itself.)

Numerical solutions computed on the two different grids, 64^3 and 128^3, show the same shapes of equilibrium configurations, and their relative differences in L_1-norm, L_2-norm, and L_∞-norm are about 0.16 when compared at a time in which significant motion has happened to the rod and the fluid, i.e., roughly half way to the stable supercoiled configuration. The parameter values used for these comparisons are as follows: $a = 0.3$, $a_3 = 0.2$, $b = 54$, $p = 4$ and $\epsilon = 10$ are kept the same; the time step durations are $\triangle t = 0.01s$ for the 64^3 grid, and $\triangle t = 0.005s$ for the 128^3 grid.

6 Conclusion

In this paper, we have generalized the immersed boundary method so that it can be used to model an immersed elastic rod with bend and twist in a viscous incompressible fluid. In the original immersed boundary method, the immersed boundary interacts with the fluid by moving at the local fluid velocity and applying force locally to the fluid. Here, the immersed boundary has an orientation as well as a position, the orientation being described by an orthonormal triad attached to each immersed boundary point. The new feature of the immersed boundary method described in this paper is that the interaction of the immersed boundary with the fluid now involves not only translation of the immersed boundary points at the local fluid velocity, but also rotation of the associated triads at the local fluid angular velocity. Similarly, we apply not only force but also torque to the fluid in which the bent twisted rod is immersed.

A key ingredient in the above scheme is a model of the bent twisted rod itself in which the triads that define the local orientation of the material are not strictly constrained to be aligned with the local tangent direction to the centerline of the rod. Instead, strong elastic forces are provided which tend to maintain such alignment without rigidly enforcing it. Similarly, we do not assume that arclength of a material segment of the rod is exactly constant, but we do provide strong elastic forces that oppose changes in the arclength of any material segment of the rod. Thus, our rod model generalizes that of Kirchhoff by replacing the constraints of the Kirchhoff rod model by penalty terms in the elastic energy that produce forces that tend to enforce those constraints. The formulation of this generalized Kirchhoff rod model is described in the Appendix.

As an example application, we consider the motion in a viscous incompressible fluid of a bent twisted rod whose centerline takes the form of a closed space curve. As is well known, such a rod has an equilibrium configuration in which its centerline is a circle, with a uniform distribution of twist. Such an equilibrium may be stable or unstable. With all other parameters held constant, the equilibrium is stable for sufficiently small twist and becomes unstable when a critical value of

the twist is reached. We have reproduced this phenomenology in the present paper, and moreover, we have used the new immersed boundary method to study what happens to the rod and the surrounding fluid in the unstable case. Here, we observe various forms of supercoiling, in which the rod eventually comes to rest in a configuration that involves self-contact.

A particular strength of the immersed boundary method proposed here, and indeed of immersed boundary methods in general, is that the contact problem is solved in a completely effortless way. There is no need to test for contact, nor to do anything special about it. The fundamental reason for this is that the points that represent the immersed boundary move in an interpolated velocity field that is continuous (and moreover has continuous first derivatives) by construction. Thus, if we consider the idealized situation of an immersed boundary method in which only the fluid grid is discretized, but the immersed boundary itself remains continuous, and in which time also remains continuous, then it is easy to see that two different immersed boundaries, or two parts of the same immersed boundary, cannot possibly cross, merely by continuity. In practice, of course, the immersed boundary is discretized and time proceeds in discrete steps, but if we take care to keep these two discretizations fine enough in relation to that of the fluid grid, then the contact problem is automatically solved. We see many instances of this in the supercoiling results of this paper, in which the bent twisted rod comes (nearly) to rest in configurations of (very near) self-contact. Indeed, it is striking in our computed results how closely the immersed boundary approaches itself without self-crossing.

We believe that the methods of this paper will find numerous applications in biological fluid dynamics. As an example, consider bacteria that swim by spinning long, thin, helical flagella. Such flagella are far from rigid. Indeed, when they all spin the same way they tend to wrap around each other forming a "superflagellum" that propels the bacterium systematically in one direction [2]. Nevertheless, their elastic resistance to bend and twist is essential to their maintenance of a helical configuration, which in turn is essential for the development of thrust. With the original immersed boundary method, it was only possible to model bacterial flagella as three-dimensional structures immersed in fluid [20]. The methods of the present paper make it possible to model bacterial flagella in a one-dimensional manner: as immersed space curves with a triad (material frame) at each point. The extreme thinness of bacterial flagella in relation to their length suggests that this is their more natural representation.

7 Acknowledgments

Our code for the simulation of the bent twisted rod immersed in fluid is built upon immersed boundary software by Nathaniel Cowen, David McQueeen, and CSP. We are indebted to David McQueen and Estarose Wolfson for the use of their visualization software and also for their technical assistance. We thank Yongsam Kim and David Swigon for useful discussions. This work was supported in part by the National Science Foundation under agreement No.0112050 at the Mathematical Biosciences Institute of Ohio State University, where SL was a postdoctoral fellow, and we thank INRIA (France) for postdoctoral support of AF.

8 APPENDIX: The unconstrained Kirchhoff rod model

We sketch here the derivation of the equilibrium equations of the unconstrained Kirchhoff rod model that is used in this paper. The state of the rod is described by a space curve $\mathbf{X}(s)$ and an associated orthonormal triad at each s, $\{\mathbf{D}^1(s), \mathbf{D}^2(s), \mathbf{D}^3(s)\}$, $0 \leq s \leq L$, where L is the unstressed length of the rod. We assume that the rod is closed on itself, forming a loop, and that $\mathbf{X}(s), \mathbf{D}^1(s), \mathbf{D}^2(s), \mathbf{D}^3(s)$ are all smoothly periodic with period L. The rod is subject to applied forces and couples denoted $\mathbf{f}(s)ds$ and $\mathbf{n}(s)ds$, respectively. The internal forces and couples transmitted across a section of the rod at s are denoted $\mathbf{F}(s)$ and $\mathbf{N}(s)$, respectively, with the sign convention that these are the forces and couples applied by the part of the rod with $s' > s$ near s to the part of the rod with $s' < s$ near s across the section of the rod at s.

Because $\{\mathbf{D}^1(s), \mathbf{D}^2(s), \mathbf{D}^3(s)\}$ is an orthonormal triad, we have the constraints

$$\mathbf{D}^i(s) \cdot \mathbf{D}^j(s) = \delta_{ij} \tag{74}$$

which we impose exactly. The sense in which our Kirchhoff rod model is unconstrained is that we do not require $\mathbf{D}^3$ to be aligned with the tangent vector to the axis of the rod $\partial\mathbf{X}/\partial s$, nor do we assume that $|\partial\mathbf{X}/\partial s| = 1$. Instead, we provide an energy penalty for deviations from these conditions, so that they tend to be maintained approximately instead of exactly. One advantage of this penalty approach is that we thereby obtain an explicit formula for the force $\mathbf{F}(s)$ that is transmitted across each section of the rod in terms of the configuration of the rod and its triad. Another advantage of the penalty formulation is that we thereby avoid imposing complicated constraints on the fluid motion in the neighborhood of the rod.

Because the transport of the triad along the rod is that of a rigid body, there must be a vector field $\mathbf{K}(s)$ such that

$$\frac{\partial \mathbf{D}^i}{\partial s} = \mathbf{K} \times \mathbf{D}^i \tag{75}$$

The components of $\mathbf{K}$ in the basis $\{\mathbf{D}^1, \mathbf{D}^2, \mathbf{D}^3\}$ are known as the *curvatures* of the rod, and a fundamental assumption of Kirchhoff rod theory is that

$$N_k(s) = a_k K_k(s) \tag{76}$$

for $k = 1, 2, 3$, where the N_k are the components of $\mathbf{N}$ in the basis $\{\mathbf{D}^1, \mathbf{D}^2, \mathbf{D}^3\}$. We assume here that the rod is homogeneous, so that the a_k do not depend on s, and moreover we assume that the triad has been set up in the *relaxed* configuration of the rod in such a way that $\mathbf{D}^1$ and $\mathbf{D}^2$ are perpendicular to the axis of the rod and aligned with the principal axes of the cross section. The constants a_1 and a_2 are called bending moduli, and the constant a_3 is the twisting modulus of the rod.

The equations of equilibrium can be derived in two ways, and comparison of the two results is very instructive. The first method is to consider force and torque balance for an arbitrary interval of the rod, say (s_1, s_2). These considerations give

$$0 = \int_{s_1}^{s_2} \mathbf{f}(s)ds + \mathbf{F}(s)|_{s_1}^{s_2} \tag{77}$$

$$0 = \int_{s_1}^{s_2} \left(\mathbf{n}(s) + (\mathbf{X}(s) \times \mathbf{f}(s))\right) ds + \left(\mathbf{N}(s) + (\mathbf{X}(s) \times \mathbf{F}(s))\right)|_{s_1}^{s_2} \tag{78}$$

In Eq. 77, we use the fundamental theorem of calculus to combine the two terms

$$0 = \int_{s_1}^{s_2} \left(\mathbf{f} + \frac{\partial \mathbf{F}}{\partial s} \right) ds \tag{79}$$

Then, since s_1 and s_2 are arbitrary,

$$0 = \mathbf{f} + \frac{\partial \mathbf{F}}{\partial s} \tag{80}$$

Eq. (78) can be manipulated in a similar way, and the result can be simplified with the help of Eq. (80). When this is done, we get

$$0 = \mathbf{n} + \frac{\partial \mathbf{N}}{\partial s} + \left(\frac{\partial \mathbf{X}}{\partial s} \times \mathbf{F} \right) \tag{81}$$

Equations (80-81) are the equilibrium equations in vector form. They implicitly involve the triad configuration $\{\mathbf{D}^1(s), \mathbf{D}^2(s), \mathbf{D}^3(s)\}$ through equations (75) and (76).

In the standard Kirchhoff rod theory, these equations are supplemented by the constraint $\partial \mathbf{X}/\partial s = \mathbf{D}^3$, which states that $\mathbf{D}^3$ is tangent to the axis of the rod, and, moreover, since $\mathbf{D}^3$ is a unit vector, that $s =$ arclength. We avoid this constraint here, and use a penalty formulation instead. This brings us to the second derivation of the equilibrium equations.

We assume that the elastic energy of the rod is given by

$$E = \frac{1}{2} \int_0^L \sum_{i=1}^{3} \left(a_i K_i^2 + b_i \left(\frac{\partial \mathbf{X}}{\partial s} \cdot \mathbf{D}^i - \delta_{3i} \right)^2 \right) ds \tag{82}$$

where the a_i have the same meaning as before, and where the new parameters b_i are the penalty constants. The parameters b_1 and b_2 may be interpreted as shear moduli, and b_3 is an extension modulus. The theory we derive here reduces to the standard theory as $b_i \to \infty$ for $i = 1, 2, 3$.

We may eliminate the K_i from Eq. (82) by solving Eq. (75) for K_i. To do this, let (i, j, k) be any cyclic permutation of $(1, 2, 3)$, and write Eq. (75) in terms of j instead of i

$$\frac{\partial \mathbf{D}^j}{\partial s} = \mathbf{K} \times \mathbf{D}^j \tag{83}$$

and then take the dot product of both sides with $\mathbf{D}^k$:

$$\frac{\partial \mathbf{D}^j}{\partial s} \cdot \mathbf{D}^k = \left(\mathbf{K} \times \mathbf{D}^j \right) \cdot \mathbf{D}^k = \mathbf{K} \cdot \left(\mathbf{D}^j \times \mathbf{D}^k \right) = \mathbf{K} \cdot \mathbf{D}^i = K_i \tag{84}$$

Thus, the elastic energy may be expressed entirely in terms of $\mathbf{X}(s), \mathbf{D}^1(s), \mathbf{D}^2(s), \mathbf{D}^3(s)$, as follows:

$$E = \frac{1}{2} \int_0^L \sum_{i=1}^{3} \left(a_i \left(\frac{\partial \mathbf{D}^j}{\partial s} \cdot \mathbf{D}^k \right)^2 + b_i \left(\frac{\partial \mathbf{X}}{\partial s} \cdot \mathbf{D}^i - \delta_{3i} \right)^2 \right) ds \tag{85}$$

Here, and throughout this Appendix, (i, j, k) always denotes a cyclic permutation of $(1, 2, 3)$.

To find the equations of equilibrium of the rod under applied forces and couples, we invoke the principle of virtual work. The work done on the rod, to first order, by the applied forces $\mathbf{f}(s)ds$

and by the applied couples $\mathbf{n}(s)ds$, during a virtual displacement $\mathbf{X} \to \mathbf{X} + \delta\mathbf{X}$ and a virtual rotation of the triad $\mathbf{D}^i \to \mathbf{D}^i + \delta\mathbf{D}^i$, where

$$\delta\mathbf{D}^i = \delta\boldsymbol{\Omega} \times \mathbf{D}^i \tag{86}$$

is given by

$$\delta\mathcal{W} = \int_0^L (\mathbf{f} \cdot \delta\mathbf{X} + \mathbf{n} \cdot \delta\boldsymbol{\Omega})\, ds \tag{87}$$

As we did previously with K, we can find the components of $\delta\boldsymbol{\Omega}$ in the basis $\{\mathbf{D}^1, \mathbf{D}^2, \mathbf{D}^3\}$ from Eq. (86). The result is

$$\delta\mathbf{D}^j \cdot \mathbf{D}^k = \delta\Omega_i \tag{88}$$

Thus Eq. (87) may be rewritten as follows:

$$\delta\mathcal{W} = \int_0^L \left(\mathbf{f} \cdot \delta\mathbf{X} + \sum_{i=1}^{3} n_i \delta\mathbf{D}^j \cdot \mathbf{D}^k \right) ds \tag{89}$$

We are now ready to apply the principle of virtual work, with Lagrange multipliers to enforce the constraints $\mathbf{D}^i \cdot \mathbf{D}^j = \delta_{ij}$. We note that these constraints are of two types ($i \neq j$ and $i = j$), with three of each type. Accordingly, we introduce the constraint function

$$E_{\mathrm{c}} = \int_0^L \sum_{i=1}^{3} \left(q_i \mathbf{D}^j \cdot \mathbf{D}^k + r_i \left(\mathbf{D}^i \cdot \mathbf{D}^i - 1 \right) \right) ds \tag{90}$$

where $q_i(s)$ and $r_i(s)$ are the six Lagrange multiplier functions. Note that $E_{\mathrm{c}} = 0$ for arbitrary $q_i(s)$ and $r_i(s)$ if and only if the constraints $\mathbf{D}^i \cdot \mathbf{D}^j = \delta_{ij}$ are satisfied.

The principle of virtual work with Lagrange multipliers now takes the following form:

$$\delta\mathcal{W} = \delta E + \delta E_{\mathrm{c}} \tag{91}$$

for arbitrary $\delta\mathbf{X}(s), \delta\mathbf{D}^1(s), \delta\mathbf{D}^2(s), \delta\mathbf{D}^3(s)$ that are smoothly periodic. We leave it as a (lengthy!) exercise for the reader to show, after eliminating the Lagrange multipliers, that the principle of virtual work implies the following two equations of equilibrium

$$0 = \mathbf{f} + \frac{\partial \mathbf{F}}{\partial s} \tag{92}$$

$$0 = n_i + a_i \frac{\partial K_i}{\partial s} + (a_k - a_j) K_j K_k + (F_k \mathbf{D}^j - F_j \mathbf{D}^k) \cdot \frac{\partial \mathbf{X}}{\partial s} \tag{93}$$

where we have made the definitions

$$F_i = b_i \left(\frac{\partial \mathbf{X}}{\partial s} \cdot \mathbf{D}^i - \delta_{3i} \right) \tag{94}$$

$$\mathbf{F} = \sum_{i=1}^{3} F_i \mathbf{D}^i \tag{95}$$

Equation (92) already agrees with the first of our equilibrium equations (80), but now we have an explicit formula for $\mathbf{F}$, Eqs. (94-95), which we did not have before. This is the main benefit of the penalty formulation.

It remains only to compare Eq. (93) with the second equilibrium equation, Eq. (81). To do so, we note the following identities, which may be verified by the reader:

$$a_i \frac{\partial K_i}{\partial s} + (a_k - a_j) K_j K_k = \frac{\partial \mathbf{N}}{\partial s} \cdot \mathbf{D}^i \tag{96}$$

$$\frac{\partial \mathbf{X}}{\partial s} \cdot \left(F_k \mathbf{D}^j - F_j \mathbf{D}^k \right) = \left(\frac{\partial \mathbf{X}}{\partial s} \times \mathbf{F} \right) \cdot \mathbf{D}^i \tag{97}$$

Thus, Eq. (93) is the i component of the vector equation

$$0 = \mathbf{n} + \frac{\partial \mathbf{N}}{\partial s} + \left(\frac{\partial \mathbf{X}}{\partial s} \times \mathbf{F} \right) \tag{98}$$

which agrees perfectly with the second equilibrium equation, Eq. (81).

Thus, we have reached the possibly surprising conclusion that the vector form of the equations of equilibrium of our unconstrained Kirchhoff rod model are *exactly* the same as the vector equations of equilibrium of the standard Kirchhoff rod, with the only difference being that in the unconstrained case we get an explicit formula for $\mathbf{F}$ to replace the missing constraint equation $\partial \mathbf{X}/\partial s = \mathbf{D}^3$.

It should be noted, however, that the two sets of equations are *not* exactly the same when resolved into components in the basis $\{\mathbf{D}^1, \mathbf{D}^2, \mathbf{D}^3\}$. This is because that basis is itself slightly rotated in the unconstrained case in comparison to its configuration in the constrained case. It turns out that the first equilibrium equation is exactly the same in the two cases despite this rotation. To see what happens to the second equilibrium equation, though, we note that Eq. (94) can be rewritten

$$\frac{\partial \mathbf{X}}{\partial s} \cdot \mathbf{D}^i = \delta_{3i} + \frac{F_i}{b_i} \tag{99}$$

and that this allows us to rewrite Eq. (93) as follows:

$$0 = n_i + a_i \frac{\partial K_i}{\partial s} + (a_k - a_j) K_j K_k + (F_k \delta_{3j} - F_j \delta_{3k}) + F_j F_k \left(\frac{1}{b_j} - \frac{1}{b_k} \right) \tag{100}$$

for $i = 1, 2, 3$, with (i, j, k) a cyclic permutation of $(1, 2, 3)$ in each case. Since the standard Kirchhoff rod model is obtained from our unconstrained rod model by letting all of the $b_i \to \infty$, we see that Eq. (100) differs from the corresponding equation in the standard case only by virtue of the last term, and moreover we see that this term can be made to vanish, not only by letting all of the b_i approach infinity, but alternatively by setting all of the b_i equal to each other, as we have done in the present work.

References

[1] S. S. Antman *Nonlinear problems of elasticity*, Springer-Verlag (1995)

[2] H.C. Berg, The rotary motor of bacterial flagella, *Annu. Rev. Biochem.*, 72:19-54 (2003)

[3] T.C. Bishop, R. Cortez, and O.O. Zhmudsky, *Investigation of bend and shear waves in a geometrically exact elastic rod model*, J. of Comput. Physics 193:642-665(2004)

[4] B.D. Coleman and D. Swigon *Supercoiled configurations with self-contact in the theory of the elastic rod model for DNA plasmids*, J. Elasticity 60, pp.171-221 (2000)

[5] B.D. Coleman, D. Swigon, and Irwin Tobias, *Elastic stability of DNA configurations. II. Supercoiled plasmids with self-contact*, Physical Review E, 61(1):759-770 (2000)

[6] B.D. Coleman and D. Swigon *Theory of self-contact in Kirchhoff rods with applications to supercoiling of knotted and unknotted DNA plasmids*, Phil. Trans. R. Soc. London. A 362, pp.1281-1299 (2004)

[7] E.H. Dill, *Kirchhoff's theory of rods*, Archives of the history of exact science 44, pp.2-23 (1992)

[8] R. Dillon, L. Fauci, and D. Gaver III, *A microscale model of bacterial swimming, chemotaxis and substrate transport*, J. Theor. Biol., 177, pp.325-340 (1995)

[9] L. Fauci and C.S. Peskin, *A computational model of aquatic animal locomotion*, J. Comput. Phys., 77, pp.85-108 (1988)

[10] A. Ferent, C.S. Peskin, and X. Wang, *Modeling a Bent Twisted Filament Immersed in Fluid*, Proc. 7th US National Congress on Computational Mechanics, Albuquerque NM (2003)

[11] A. L. Fogelson, *A mathematical model and numerical method for studying platelet adhesion and aggregation during blood clotting*, J. Comput. Phys., 56 pp. 111–134 (1984)

[12] E. Givelberg, *Modelling Elastic Shells Immersed in Fluid*, Ph.D. thesis, Mathematics, New York University (1997); available online at http://www.umi.com/hp/Products/DisExpress.html, order number 9808292.

[13] R.E. Goldstein, T.R. Powers, and C.H. Wiggins *Viscous Nonlinear Dynamics of Twist and Writhe* Physical Review Letters 80, 5232 (1998)

[14] A. Goriely and M. Tabor, *Nonlinear dynamics of filaments I. Dynamical instabilities*, Physica D 105:20-44 (1997)

[15] A. Goriely and M. Tabor, *Nonlinear dynamics of filaments II. Nonlinear analysis*, Physica D 105:45-61 (1997)

[16] A. Goriely and M. Tabor, *The Nonlinear dynamics of filaments*, Nonliear Dynamics 21:101-133 (2000)

[17] K.A. Hoffman, R.S. Manning, J.H. Maddocks *Link, twist, energy, and the stability of DNA minicircles*, Biopolymers, 70(2): 145-157 (2003)

[18] E. Jung and C.S. Peskin, *Two-dimensional simulations of valveless pumping using the immersed boundary method*, SIAM J. Sci. Comput., 23 pp.19-45 (2001)

[19] I. Klapper, *Biological applications of the dynamics of twisted elastic rods*, Journal of Computational Physics 125, pp.325-337 (1996)

[20] S. Lim and C.S. Peskin, *Simulations of the whirling instability by the immersed boundary method*, SIAM J. Sci. Comput. 25:2066-2083(2004)

[21] A.E. Love, *A treatise on the mathematical theory of elasticity*, Cambridge University Press, Cambridge (1892)

[22] N.H. Mendelson *Helical growth of Bacillus subtilis: A new model of cell growth* Proc. NAtl. Acad. Sci., 73:1740-1744 (1976)

[23] N.H. Mendelson *Bacterial growth and division: genes, structures, forces and clocks*, Microbiological Reviews, 46:341-375 (1982)

[24] N.H. Mendelson, J.J. Thwaites, J.O. Kessler, and C. Li, *Mechanics of bacterial macrofiber initiation*, Journal of Bacteriology, 177:7060-7069 (1995)

[25] C.S. Peskin, *The immersed boundary method*, in Acta Numerica, Cambridge University Press, Cambridge, UK, pp.1-39 (2002)

[26] C. S. Peskin *Flow patterns around heart valves: A numerical method*, J. Comput. Phys., 10, pp.252-271 (1972)

[27] C. S. Peskin *Numerical analysis of blood flow in the heart*, J. Comput. Phys., 25, pp.220–252 (1977)

[28] C. S. Peskin and D. M. McQueen, *Fluid dynamics of the heart and its valves*, in Case Studies in Mathematical Modeling: Ecology, Physiology, and Cell Biology, H. G. Othmer, F. R. Adler, M. A. Lewis, and J. C. Dallon, eds., Prentice-Hall, Englewood Cliffs, NJ, pp.309-337 (1996)

[29] T.R. Strick, J.F. Allemand, D. Bensimon, and V. Croquette, *Behavior of supercoiled DNA*, Biophysical J. 74:2016-2028(1998)

[30] T. Schlick and W.K. Olson, *Trefoil Knotting Revealed by Molecular Dynamics Simulations of Supercoiled DNA*, Science, 257:1110-1115 (1992)

[31] Tamar Schlick, *Modeling superhelical DNA : recent analytical and dynamics approaches*, Current Opinion in Structural Biology 5:245-262(1995)

[32] C.W. Wolgemuth, R.E. Goldstein, and T.R. Powers, *Dynamic supercoiling bifurcations of growing elastic filaments*, Physica D 190:266-289(2004)

[33] Y. Yang, I. Tobias, and W.K. Olson, *Finite element analysis of DNA supercoiling*, J. Chem. Phys. 98(2):1673-1686(1993)

[34] L. Zhu and C. S. Peskin, *Simulation of a flapping flexible filament in a flowing soap film by the immersed boundary method*, J. Comput. Phys., 179 pp.452-468 (2002)